Journal of Dental Research
2020, Vol. 99(3) 311–319

DOI: 10.1177/0022034519897607
journals.sagepub.com/home/jdr

Epithelial *Wnt10a* Is Essential for Tooth Root Furcation Morphogenesis

M. Yu[1*], Y. Liu[1*], Y. Wang[1], S.W. Wong[2], J. Wu[1], H. Liu[1], H. Feng[1], and D. Han[1]

Abstract

WNT10A (Wingless-type MMTV integration site family, member 10A) plays a crucial role in tooth development, and patients with biallelic *WNT10A* mutation and mice lacking *Wnt10a* show taurodontism. However, whether epithelial or mesenchymal *WNT10A* controls the initiation of the root furcation formation remains unclear, and the functional significance of *WNT10A* in regulating root morphogenesis has not been clarified. Here, we investigated how *Wnt10a* affects tooth root development by generating different tissue-specific *Wnt10a* conditional knockout mice. *Wnt10a* knockout in the whole tissue (*EIIa-Cre;Wnt10a*$^{flox/flox}$) and in dental epithelium (*K14-Cre;Wnt10a*$^{flox/flox}$) led to an absence of or apically located root furcation in molars of mice, a phenotype that resembled taurodontism. An RNAscope analysis showed that the dynamic epithelial and mesenchymal *Wnt10a* expression pattern occurred during root development. Immunofluorescent staining of E-cadherin and EdU revealed decreased epithelial cell proliferation at the cervical region of the molar in *K14-Cre;Wnt10a*$^{flox/flox}$ mice at postnatal day 0 (PN0), just before the initiation of root morphogenesis. Interestingly, we found increased pulpal mesenchymal cell proliferation in the presumptive root furcating region of the molar in *K14-Cre;Wnt10a*$^{flox/flox}$ mice at PN4 and PN7. RNA-seq indicated that among the Wnt ligands with high endogenous expression levels in molars, *Wnt4* was increased after epithelial knockout of *Wnt10a*. The RNAscope assay confirmed that the expression of *Wnt4* and *Axin2* in the dental papilla of the presumptive root furcating region, where dental pulp overgrowth occurred, was increased in *K14-Cre;Wnt10a*$^{flox/flox}$ molars. Furthermore, after suppression of the elevated *Wnt4* level in *K14-Cre;Wnt10a*$^{flox/flox}$ molars by *Wnt4* shRNA adenovirus and kidney capsule grafts, the root furcation defect was partially rescued. Taken together, our study provides the first in vivo evidence that epithelial *Wnt10a* guides root furcation formation and plays a crucial role in controlling the organized proliferation of adjacent mesenchymal cells by regulating proper *Wnt4* expression during root furcation morphogenesis.

Keywords: taurodontism, tooth abnormalities, cell proliferation, tooth root, development, Wnt signaling

Introduction

The tooth root is a unique and functional part of the dentition because it anchors teeth to the jaw bones (Li et al. 2017). The molars have multiple roots with furcation in between that allows for the transmittal and balance of occlusal forces to the alveolar bones during mastication (Wu et al. 2018). The loss of roots and defects in the root size and shape lead to reduced alveolar bone support and perturbed tooth function. Therefore, understanding the root development process and the regulatory mechanism is a prerequisite for studying the tooth root. Tooth root development is an intricate process, and similar to crown development, it is regulated by reciprocal interactions between the dental epithelium and mesenchyme (Huang and Chai 2012). Several highly conserved signaling pathways mediate the epithelial-mesenchymal interactions during root development, including the transforming growth factor β, hedgehog, and Wnt/β-catenin signaling pathways (van Genderen et al. 1994; Thesleff 2003; Li et al. 2017).

WNT10A is a ligand in the Wnt/β-catenin pathway. Recent evidences have shown that *WNT10A* mutations play a major pathogenic role in human tooth agenesis (Kantaputra and Sripathomsawat 2011; van den Boogaard et al. 2012; He et al. 2013; Song et al. 2014; Yu, Wong, et al. 2019). *WNT10A* mutations could cause nonsyndromic oligodontia, odonto-onycho-dermal dysplasia (OMIM#257980), and Schöpf-Schulz-Passarge syndrome (OMIM#224750; Adaimy et al. 2007; Petrof et al. 2011). We first reported that patients with odonto-onycho-dermal

[1]Department of Prosthodontics, Peking University School and Hospital of Stomatology & National Clinical Research Center for Oral Diseases & National Engineering Laboratory for Digital and Material Technology of Stomatology & Beijing Key Laboratory of Digital Stomatology, Beijing, China
[2]Division of Comprehensive Oral Care–Periodontology, Adams School of Dentistry, University of North Carolina at Chapel Hill, Chapel Hill, NC, USA
*Authors contributing equally to this article.

A supplemental appendix to this article is available online.

Corresponding Author:
D. Han, Department of Prosthodontics, Peking University School and Hospital of Stomatology & National Clinical Research Center for Oral Diseases & National Engineering Laboratory for Digital and Material Technology of Stomatology & Beijing Key Laboratory of Digital Stomatology, 22 Zhongguancun South Avenue, Beijing 100081, China.
Email: donghan@bjmu.edu.cn

dysplasia and biallelic *WNT10A* mutations had typical taurodontism, a condition characterized by defects in tooth root furcation of deciduous molars (Yu, Liu, et al. 2019). Moreover, *Wnt10a*$^{-/-}$ mice show taurodontism (Yang et al. 2015; Xu et al. 2017), indicating that there must be a significant role of *Wnt10a* in tooth root morphogenesis.

Wnt10a expression can be observed in the epithelium and mesenchyme throughout the entire processes of pre- and postnatal tooth development. *Wnt10a* is strongly expressed in the dental epithelium at the bud stage (embryonic day 13.5 [E13.5]) and cap stage (E14.5; Dassule and McMahon 1998), whereas its expression shifts from secondary enamel knots to the underlying mesenchymal cells at E16 (Yamashiro et al. 2007). *Wnt10a* expression is mainly presented in the preodontoblasts and adheres to Hertwig's epithelial root sheath (HERS) during root development (Yamashiro et al. 2007). However, *Wnt10a* expression in the epithelial or HERS cells during root development was not carefully observed or mentioned. Although considerable evidence has shown the strong link between *Wnt10a* and root morphogenesis, whether epithelial or mesenchymal *Wnt10a* controls the initiation of root furcation remains unclear, and the functional significance of *Wnt10a* in regulating root morphogenesis has not been confirmed.

In the present study, we explored the role of *Wnt10a* in root development by establishing murine models via the conditional deletion of the *Wnt10a* gene in the whole body, dental epithelium, and dental mesenchyme and investigating the root morphology of the mandibular molars. We found that *K14-Cre;Wnt10a*$^{flox/flox}$, rather than *Wnt1-Cre;Wnt10a*$^{flox/flox}$, developed taurodontism in the molars. Knockout of epithelial *Wnt10a* resulted in 1) decreased proliferation of apical epithelial cells before root initiation and increased pulpal mesenchymal cell proliferation, 2) which is associated with the compensatory elevation of *Wnt4* and upregulated the expression of *Axin2* in the presumptive furcation region during root development. Additionally, adenovirus-mediated knockdown of *Wnt4* in the first molars partially rescued the taurodontism defect in *K14-Cre;Wnt10a*$^{flox/flox}$ mice. Our findings demonstrate that epithelial *Wnt10a* is specifically required during root furcation formation and crucial for the proper proliferation of epithelial and mesenchymal cells in the furcation region during root morphogenesis.

Materials and Methods

Mouse Models

Wnt10a$^{flox/flox}$ mice on a C57BL/6J background were generated by Cyagen Biosciences Inc. *EIIa-Cre* (Lakso et al. 1996), *K14-Cre* (Byrne et al. 1994), and *Wnt1-Cre* (Brault et al. 2001) mice were crossed with *Wnt10a*$^{flox/flox}$ mice to generate the different conditional knockout mice. All animal experiments were approved by the Ethics Committee of the Peking University Health Science Center (PKUSSIRB-201736082).

Micro–computed tomography Analysis

The parameters of the Inveon MM system (Gantry-STD CT; Siemens) were set as follows: voltage of 60 kV, current of 220 mA, exposure time of 1500 ms, and effective pixel size of 8.89 μm. Sagittal images of the mandibles from 3-wk-old *K14-Cre;Wnt10a*$^{flox/flox}$ and *Wnt10a*$^{flox/flox}$ mice were captured with Inveon software. The slices through the furcation of the first mandibular molar were chosen for the quantitative analysis.

Histologic Analysis

For hematoxylin and eosin staining, mandibles from *K14-Cre;Wnt10a*$^{flox/flox}$ and *Wnt10a*$^{flox/flox}$ mice at postnatal day 0 (PN0), PN4, PN7, PN14, and PN28 ($n = 3$ per stage) were processed and stained according to standard procedures.

Immunostaining

For E-cadherin and 5-ethynyl-2′-deoxyuridine (EdU) dual immunofluorescence labeling, mice at PN0, PN4, and PN7 ($n = 3$ per stage) were sacrificed 6 h after intraperitoneal injection with EdU (5 mg/kg; RiboBio), and the incorporated EdU was detectable by the Click-iT Apollo 567 Stain Kit (RiboBio).

RNA-seq and Data Analysis

Three pairs of biological replicates (pooling 4 first mandibular molars as 1 sample) of the RNA samples were collected from *K14-Cre;Wnt10a*$^{flox/flox}$ and *Wnt10a*$^{flox/flox}$ mice at PN4. Samples were sent to the Beijing Genomic Institution for mRNA enrichment, cDNA library construction, and sequencing with the BGISEQ-500 platform. SOAPnuke was employed to filter low-quality reads and obtain high-quality clean reads. The alignment was acquired by comparing the clean reads and the reference gene sequence with Bowtie-2 software. The gene expression levels were counted and normalized to fragments per kilobase of exon model per million mapped reads by RESM software. The $\log_2$-fold changes and $-\log_{10}$ ($P \leq 0.05$) of the Wnt signaling–related genes were integrated to create the volcano plot and the heat map. The list of differential expression genes was generated by the combination of the absolute value of log2 ratio ≥ 0.1 (*K14-Cre;Wnt10a*$^{flox/flox}$/ *Wnt10a*$^{flox/flox}$) and Q value ≤ 0.001 (*Wnt10a*$^{flox/flox}$-vs-*K14-Cre;Wnt10a*$^{flox/flox}$) with the Beijing Genomic Institution bioinformatics platform. The expression profiles were deposited in the Gene Expression Omnibus database (GSE125893).

RNAscope In Situ RNA Analysis

The detection of *Wnt10a, Wnt4*, and *Axin2* signals was performed by RNAscope analysis with RNAscope 2.5 HD Reagent Kit–Red (Advanced Cell Diagnostics) according to the manufacturer's procedure as previously described (Wang et al. 2012).

Adenovirus Infection and Kidney Capsule Transplantation

The pDC316-ZsGreen-shRNA vector was used to generate shRNA against the mouse *Wnt4* gene (NM_009523.2). Recombinant adenoviruses of Ad-ZsGreen-shRNA-mWnt4-1, mWnt4-2, mWnt4-3 (Ad-Wnt4 group), and Ad-ZsGreen-shRNA (Ad-control group) were constructed by Likely Biotechnology via the AdMax system. To verify the extent of adenovirus infection, the first mandibular molars ($n = 3$) from PN4 *Wnt10a*$^{flox/flox}$ mice were dissected and infected with Ad-control and Ad-Wnt4, and the cryosections of kidney capsule transplantation after 7-d culture were examined. For the rescue experiment, kidney capsule transplantation was carried out as previously described (Li et al. 2011).

Results

Epithelial-Wnt10a but Not Mesenchymal-Wnt10a Is Crucial for the Proper Formation of Root Furcation

To discuss whether epithelial or mesenchymal *Wnt10a* controls the formation of root furcation, we generated *EIIa-Cre;Wnt10a*$^{flox/flox}$, *K14-Cre;Wnt10a*$^{flox/flox}$, and *Wnt1-Cre;Wnt10a*$^{flox/flox}$ mice (Appendix Figs. 1, 2). Then, we performed a micro–computed tomography analysis to identify the postnatal root morphology in 3 specific *Wnt10a* conditional knockout mice. We found that *EIIa-Cre;Wnt10a*$^{flox/flox}$ and *K14-Cre;Wnt10a*$^{flox/flox}$ mice developed an absence of or apically located root furcation, a higher pulp chamber, and a larger pulp cavity in molars (Fig. 1A–C), whereas the root furcation and root numbers of *Wnt1-Cre;Wnt10a*$^{flox/flox}$ mice were almost unaffected (Fig. 1D). Particularly, a comparison with the *Wnt10a*$^{flox/flox}$ mice showed that the ratio of pulp chamber height to root length increased by 6.8-fold in *EIIa-Cre;Wnt10a*$^{flox/flox}$ mice ($P < 0.0001$) and 7-fold in *K14-Cre;Wnt10a*$^{flox/flox}$ mice ($P < 0.0001$; Fig. 1E). Therefore, the characteristics observed in *EIIa-Cre;Wnt10a*$^{flox/flox}$ and *K14-Cre;Wnt10a*$^{flox/flox}$ mice phenocopied the taurodontism of human with the biallelic *WNT10A* mutation.

Ablation of Wnt10a in Epithelium Results in the Failure of Pulp Chamber Floor Formation in Molars

To further address the role of epithelial *Wnt10a* during root furcation development, we performed hematoxylin and eosin staining of the first mandibular molars at key development time points in *Wnt10a*$^{flox/flox}$ and *K14-Cre;Wnt10a*$^{flox/flox}$ mice. At PN0, no significant differences were observed between the *K14-Cre;Wnt10a*$^{flox/flox}$ and *Wnt10a*$^{flox/flox}$ molars (Fig. 2A, B). At PN4, the tooth crown of *Wnt10a*$^{flox/flox}$ mice had grown to its full size; HERS had formed; and root had initiated at the apical papilla (Fig. 2C, C′). Specifically, the mandibular first molar of *Wnt10a*$^{flox/flox}$ mice already exhibited a horizontal elongation of HERS from the buccal and lingual sides at the root furcation region (Fig. 2M, M′). However, in *K14-Cre;Wnt10a*$^{flox/flox}$ mice, the growth retardation of the epithelium toward the center from the buccal and lingual sides was apparent, and the horizontal elongation of epithelium was not observed (Figs. 2D, D′, N, N′). At PN7, more remarkable morphologic differences were found between the 2 groups. In *Wnt10a*$^{flox/flox}$ mice, the apical papilla began to grow apically, and the HERS in the furcation was visible (Fig. 2E, E′, Q, Q′). However, in *K14-Cre;Wnt10a*$^{flox/flox}$ mice, the epithelial pulp chamber floor failed to form in the putative furcation (Fig. 2F, F′, R, R′). At PN14, the root continued to grow apically, and at PN28, the molars had fully erupted into the oral cavity. The first mandibular molars in *Wnt10a*$^{flox/flox}$ mice formed a typical root furcation (Fig. 2G, I), while the root furcation was extremely apically located and inapparent in *K14-Cre;Wnt10a*$^{flox/flox}$ mice (Fig. 2H, J). The schematic diagram showed the section orientation and the mesial (nonfurcation) and furcation regions that we described earlier (Fig. 2S–X). Our data demonstrate that ablation of *Wnt10a* in dental epithelium results in taurodontism and impairs root furcation morphogenesis.

Loss of Wnt10a in the Epithelium Results in the Decreased Proliferation of Epithelial Cells and Increased Proliferation of Mesenchymal Cells in the Presumptive Root Furcating Region

To demonstrate the functional significance of *Wnt10a* during root development, we performed an RNAscope assay to observe the *Wnt10a* expression pattern at serial developmental stages. At E18.5, *Wnt10a* mRNA was expressed in the dental epithelium and mesenchyme of the crown (Figs. 3A, A′). At PN2, immediately before the emergence of HERS, *Wnt10a* was expressed in the epithelial and adjacent mesenchymal cells at the cervical region (Fig. 3B, B′). At PN6, when HERS elongated horizontally at the central part of tooth, *Wnt10a* was expressed in HERS and adjacent dental papilla cells of the root furcating region (Fig. 3C, C′). At PN9, when the pulp chamber floor formed, *Wnt10a* expression was aggregated in the odontoblasts at the root furcation and the surrounding dental follicle cells, although it was hardly detected in the epithelial cells (Fig. 3D, D′). At PN11 and PN14, the expression of *Wnt10a* had almost disappeared in the dental pulp and alveolar bone beneath the root furcation (Fig. 3E, E′, F, F′). This dynamic expression pattern suggested that *Wnt10a* might play a unique role during root furcation development.

To investigate the cellular mechanism responsible for taurodontism in *K14-Cre;Wnt10a*$^{flox/flox}$ mice, we examined cell proliferation and apoptosis. E-cadherin, an epithelial cell adhesion marker, was used to distinguish the dental mesenchyme from the dental epithelium (Verstraeten et al. 2010). At PN0, EdU-positive cells could be seen in the dental epithelium and mesenchyme of the cervical loop (Fig. 3G_1–G_3). A quantitative analysis of the EdU+/DAPI+ nuclei rate showed that proliferation of dental epithelial cells in the cervical loop of the presumptive root furcating region was significantly decreased in *K14-Cre;Wnt10a*$^{flox/flox}$ mice as compared with *Wnt10a*$^{flox/flox}$

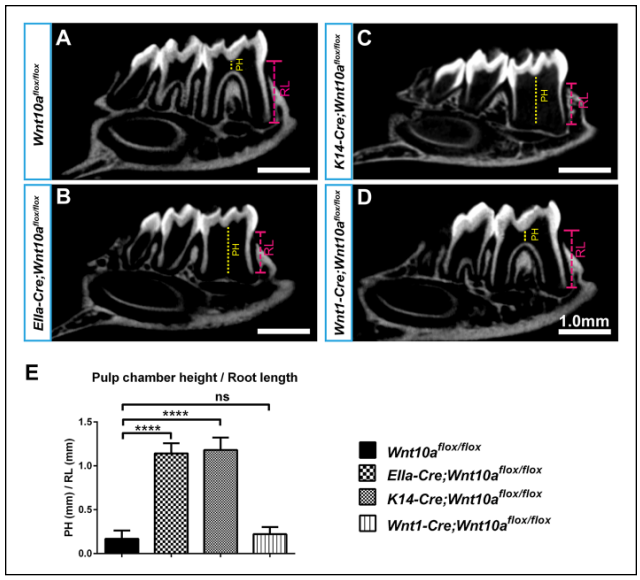

Figure 1. Micro–computed tomography (μCT) analysis of mandibles from *Wnt10a* knockout and control mice. (**A–D**) Representative μCT images of the mandibles from 3-wk-old *Wnt10a*$^{flox/flox}$, *Ella-Cre;Wnt10a*$^{flox/flox}$, *K14-Cre;Wnt10a*$^{flox/flox}$, and *Wnt1-Cre;Wnt10a*$^{flox/flox}$ mice. (**E**) Quantification of the pulp chamber height / mesial tooth root length of the first mandibular molars (M1) from μCT. $n = 3$ per group. ****$P < 0.0001$. ns, no statistic difference. Values are presented as the mean ± SD. PH, pulp chamber height; RL, root length. Scale bar: 1.0 mm.

mice (Fig. 3G_1–G_3, H_1–H_3, M). Interestingly, when HERS elongated horizontally at PN4, EdU-positive cells were mainly found in the dental papilla and dental follicle adhering to HERS rather than in the HERS cells (Fig. 3I_1–I_3). A quantitative analysis showed that the proliferation of dental papilla cells in the furcation was significantly increased in the *K14-Cre;Wnt10a*$^{flox/flox}$ mice as compared with the *Wnt10a*$^{flox/flox}$ mice at PN4 (Fig. 3I_1–I_3, J_1–J_3, N) and PN7 (Fig. 3K_1–K_3, L_1–L_3, N). However, significant differences were not observed in the proliferation of dental follicle cells surrounding the furcation between *K14-Cre;Wnt10a*$^{flox/flox}$ and *Wnt10a*$^{flox/flox}$ mice at PN4 and PN7 (Fig. 3I_2–J_2, K_2–L_2, O). Furthermore, we found that apoptosis mainly occurred in the occlusal region of the enamel organ and dental pulp beneath the cusps, while apoptosis was hardly detected in presumptive root furcating region in *Wnt10a*$^{flox/flox}$ and *K14-Cre;Wnt10a*$^{flox/flox}$ molar germs at PN2 (Appendix Fig. 3). Therefore, our data indicate that epithelial *Wnt10a* regulates the organized proliferation of epithelial and dental pulpal mesenchymal cells in the furcation region during root development.

Ablation of Epithelial Wnt10a Results in the Compensatory Elevation of Wnt4 and Upregulated Activation of Axin2 in Dental Papilla

Wnt ligands are essential for cell proliferation during tooth development; therefore, we hypothesized that other Wnt ligands may be upregulated to compensate for the loss of epithelial *Wnt10a*. To test this hypothesis, we first explored the activity of canonical Wnt signaling by an RNAscope analysis of *Axin2*, a Wnt pathway activation readout, in *Wnt10a*$^{flox/flox}$ and *K14-Cre;Wnt10a*$^{flox/flox}$ first mandibular molars at PN4. We found an elevated *Axin2* signal in the mesenchyme of dental papilla adjacent to the epithelium of the presumptive root furcating region in *K14-Cre;Wnt10a*$^{flox/flox}$ molars as compared with the *Wnt10a*$^{flox/flox}$ molars, where increased cell proliferation occurred as mentioned earlier (Fig. 4A, B).

To precisely define the expression profiles of Wnt ligands during root furcation morphogenesis, we performed an RNA-seq analysis in the first mandibular molars of *Wnt10a*$^{flox/flox}$ and *K14-Cre;Wnt10a*$^{flox/flox}$ mice at PN4. The results identified 26 differentially expressed Wnt pathway–associated genes between 2 groups: 7 genes were upregulated and 19 genes were downregulated in *K14-Cre;Wnt10a*$^{flox/flox}$ mice ($P < 0.05$; Fig. 4C). The volcano plot analysis showed that *Wnt5a* and *Wnt7b* were significantly downregulated and *Wnt4* was significantly upregulated in *K14-Cre;Wnt10a*$^{flox/flox}$ mice (Fig. 4C). Moreover, the heat map and RT-qPCR (reverse transcription quantitative polymerase chain reaction) of Wnt ligands demonstrated that the endogenous expression level of *Wnt4* was relatively high in *Wnt10a*$^{flox/flox}$ molars and *Wnt4* was significantly increased in *K14-Cre;Wnt10a*$^{flox/flox}$ molars (Fig. 4D–F).

Given these results, we hypothesized that the upregulation of *Wnt4* contributed to the increased dental pulp cell proliferation after epithelial-*Wnt10a* knockout. To test that, we investigated the *Wnt4* expression in first mandibular molars of *Wnt10a*$^{flox/flox}$ and *K14-Cre;Wnt10a*$^{flox/flox}$ mice by RNAscope. In *Wnt10a*$^{flox/flox}$ mice, *Wnt4* was mainly expressed in the HERS cells (Fig. 5A). However, in *K14-Cre;Wnt10a*$^{flox/flox}$ mice, increased *Wnt4* expression occurred in the dental papilla mesenchymal cells of the presumptive root furcating region (Fig. 5B).

Partial Rescue of Taurodont Defects in K14-Cre;Wnt10a$^{flox/flox}$ *Mice after Wnt4 Silencing*

To test the hypothesis that the dental papilla mesenchymal *Wnt4* acts downstream of Wnt10a-mediated Wnt/β-catenin signaling in the epithelium to control root furcation morphogenesis, we employed rescue experiments with adenovirus-mediated *Wnt4* knockdown in PN4 mouse molars and kidney capsule transplantation. After 24 h of adenovirus infection, Western blotting results showed that, when compared with the control-shRNA infected molars, Wnt4 expression was decreased by as much as 80% in the *Wnt4*-shRNA infected molars ($P < 0.001$; Appendix Fig. 4). After 7-d culture in kidney capsule, fluorescence examination was performed to identify the location and extent of adenovirus, and the results showed that the entire dental epithelium and most parts of the mesenchyme were green fluorescent protein (GFP) positive, indicating that control-shRNA and *Wnt4*-shRNA infection was successful (Appendix Fig. 5). After 18 d of growth in the kidney capsule, the micro–computed tomography results demonstrated that the control-shRNA-infected *Wnt10a*$^{flox/flox}$ molars were all well developed ($n = 8$) with a normal root morphology, a typical furcation structure in

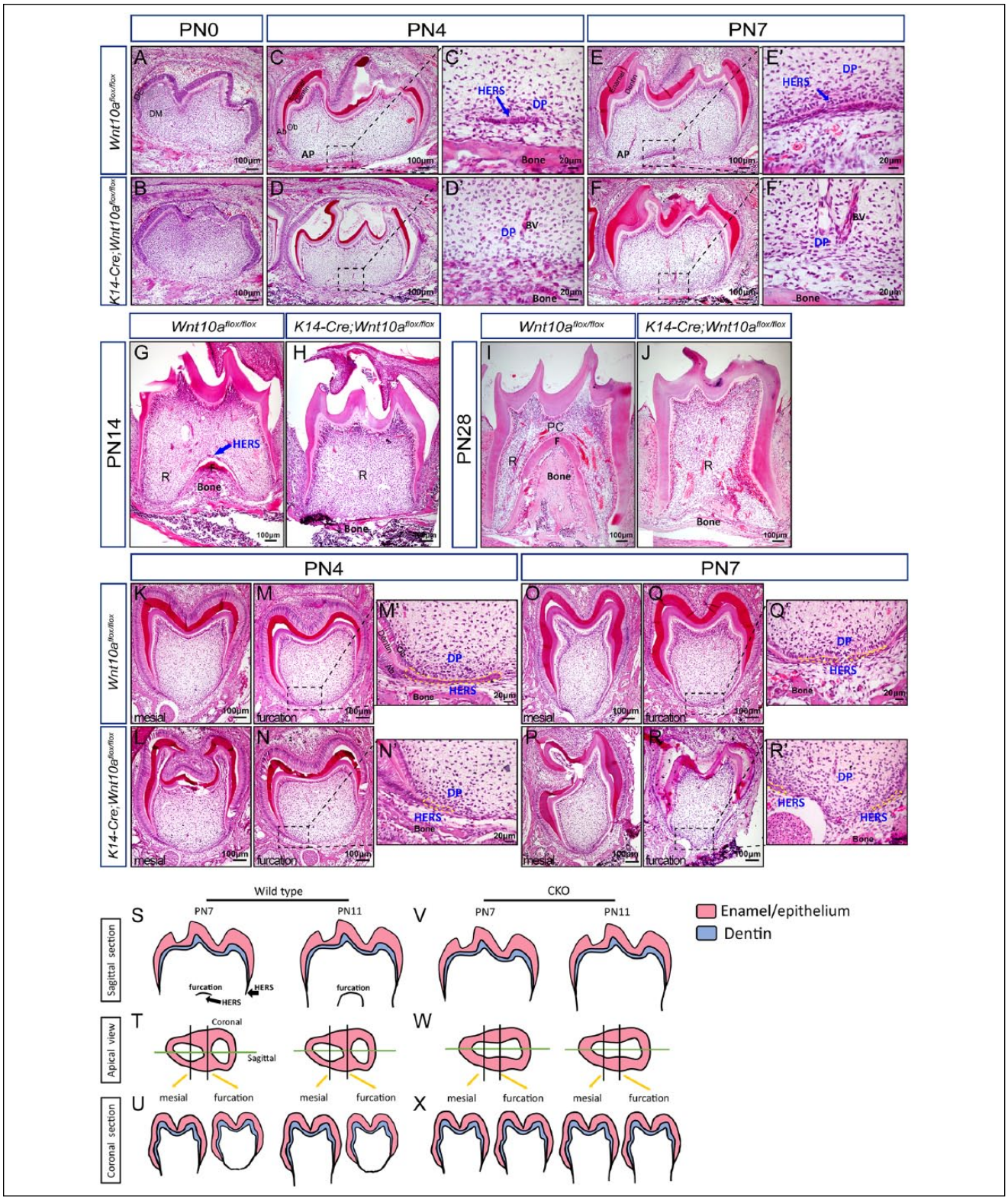

Figure 2. Comparison of the tooth histology during postnatal root development of the first mandibular molar. (**A–J**) Representative sagittal images of hematoxylin and eosin–stained M1 from *Wnt10a*$^{flox/flox}$ mice and *K14-Cre;Wnt10a*$^{flox/flox}$ mice at PN0, PN4, PN7, PN14, and PN28. Scale bars: 100 μm. (C′–F′) Higher magnification of the region where root furcation would form at PN4 and PN7, with blue arrows indicating HERS cells. Scale bars: 20 μm. (**K–R**) Coronal images of the mesial root and central root furcation region of M1 from *Wnt10a*$^{flox/flox}$ and *K14-Cre;Wnt10a*$^{flox/flox}$ mice at PN4 and PN7. Scale bars: 100 μm. (M′, N′, Q′, R′) Higher-magnification fields of the representative root furcation region are outlined with a black dashed line at PN4 and PN7. Yellow dashed line circles the HERS cells. Scale bars: 20 μm. (**S–U**) Schematic diagrams of normal tooth root furcation development in sagittal view, apical view, and coronal view at PN7 and PN11. (**V–X**) Schematic diagrams of taurodontism formation in sagittal view, apical view, and coronal view at PN7 and PN11. Dentin is shown in blue; epithelium and enamel are shown in pink. Ab, ameloblast; AP, apical papilla; BV, blood vessel; DE, dental epithelium; DM, dental mesenchyme; DP, dental pulp; F, furcation; HERS, Hertwig's epithelial root sheath; M1, first mandibular molar; Ob, odontoblast; PC, pulp chamber; PN, postnatal day; R, root.

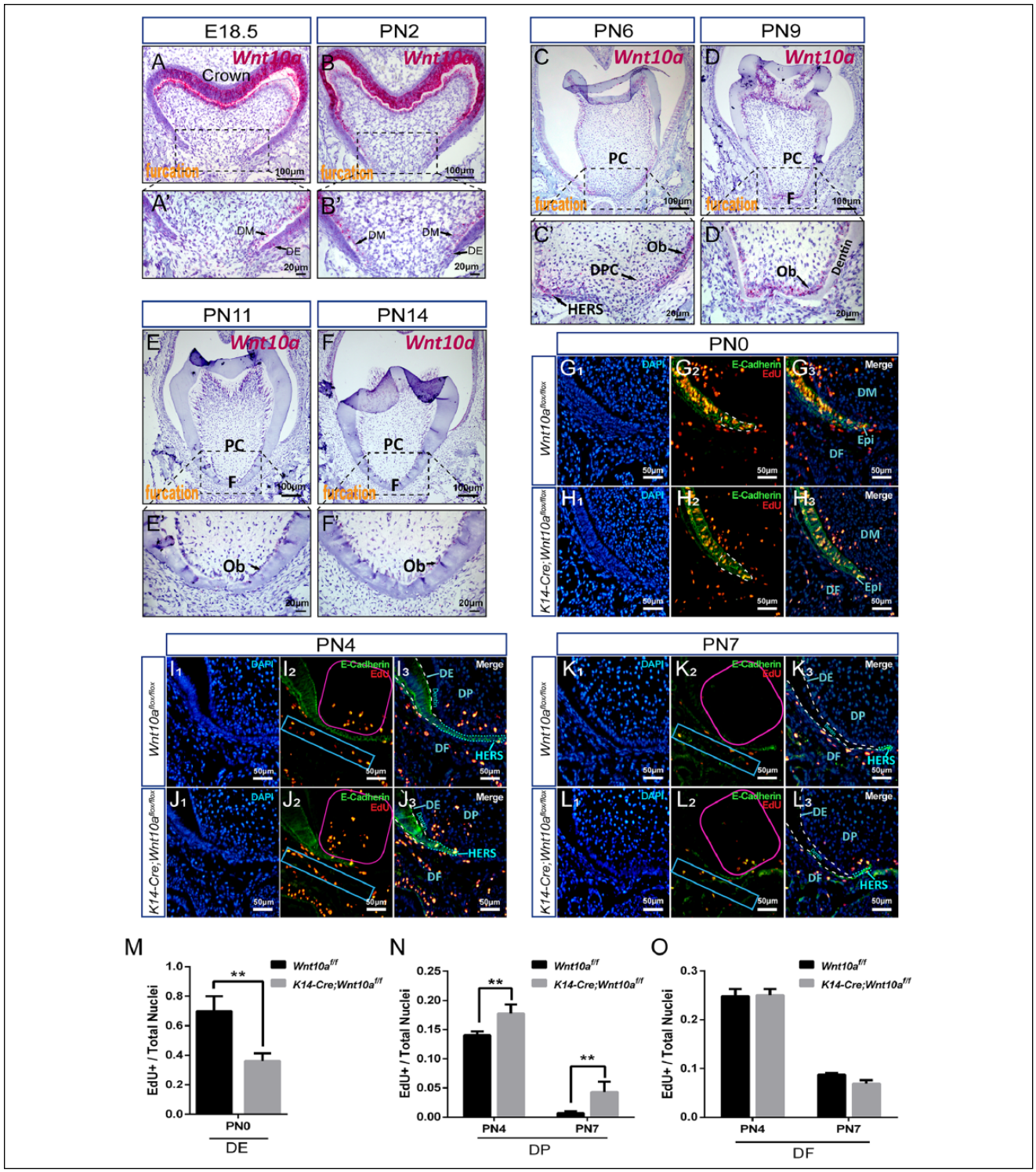

Figure 3. Expression pattern of *Wnt10a* during tooth root development and altered proliferation in dental epithelial and mesenchymal cells of *K14-Cre;Wnt10a*$^{flox/flox}$ mice. (**A–F**) RNAscope in situ hybridization of *Wnt10a*, with positive staining in red dots, on coronal sections of the central root furcation region of M1 from wild-type mice at E18.5, PN2, PN6, PN9, PN11, and PN14. Scale bars: 100 μm. (A′–F′) Higher magnifications of the bottom of the pulp chamber are outlined with a black dashed line in the images above. Scale bars: 20 μm. (**G**$_{1-3}$**–L**$_{1-3}$) Combinations of the 3 fluorescence signals (anti-E-cadherin in green, EdU in red, and DAPI in blue) show the proliferation of dental epithelial and mesenchymal cells in the labial half of the central root furcation region of the first mandibular molars from *Wnt10a*$^{flox/flox}$ mice and *K14-Cre;Wnt10a*$^{flox/flox}$ mice. White and cyan dashed lines circle the dental epithelium and the HERS, respectively. Pink solid line outlines the dental pulp adjacent to the HERS cells in the root furcation region for quantification. Blue solid line outlines the dental follicle cells in the root furcation region for quantification. Scale bars: 50 μm. (**M**) Ratios of EdU$^+$/DAPI$^+$ cells representing the dental epithelial cell proliferation rate in the region where HERS would form at PN0. (**N**) Ratios of EdU$^+$/DAPI$^+$ cells representing the dental mesenchymal cell proliferation rate from the outlined regions adjacent to the HERS cells in the dental pulp at PN4 and PN7. (**O**) Ratios of EdU$^+$/DAPI$^+$ cells representing the dental follicle cell proliferation activity in the root furcation region at PN4 and PN7. $n = 3$ per group. DE, dental epithelium; DF, dental follicle; DM, dental mesenchyme; DP, dental pulp; DPC, dental pulpal cells; E18.5, embryonic day 18.5; Epi, epithelium; F, furcation; HERS, Hertwig's epithelial root sheath; M1, first mandibular molar; Ob, odontoblasts; PC, pulp chamber; PN, postnatal day. Values are presented as mean ± SD. $^{**}P < 0.01$.

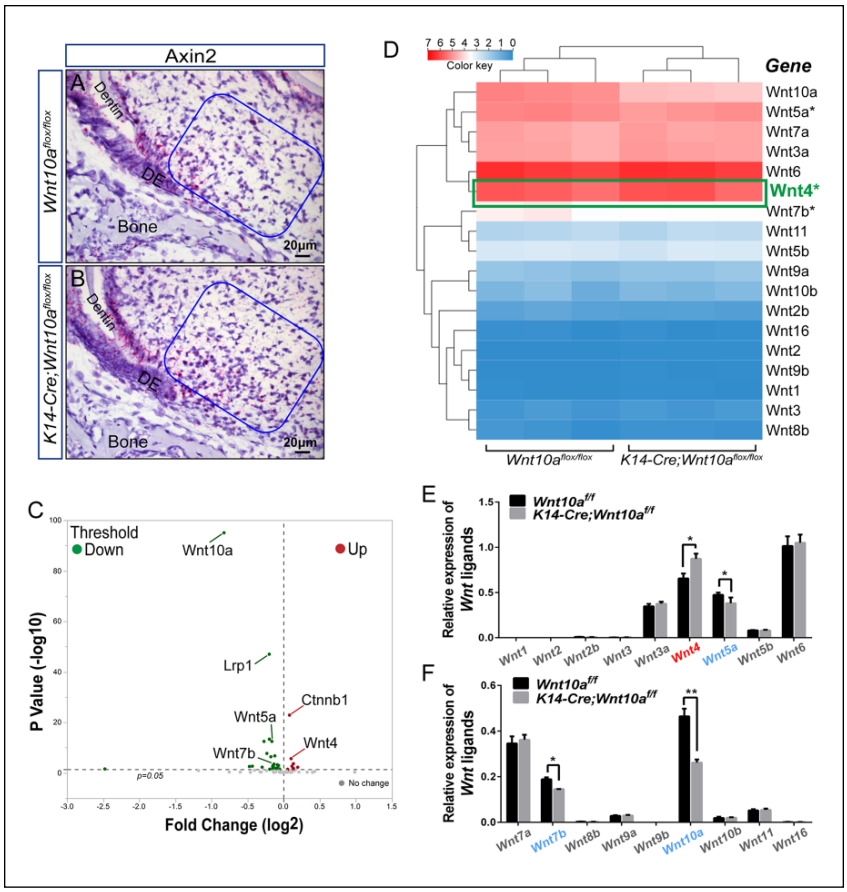

Figure 4. Elevated Wnt/β-catenin activity in the pulp of furcation region of the *K14-Cre;Wnt10a*$^{flox/flox}$ mice and RNA-sequencing results of Wnt genes. (**A**, **B**) RNAscope in situ hybridization of *Axin2*, with positive staining in red, on coronal section in the furcation region of M1 from *Wnt10a*$^{flox/flox}$ mice and *K14-Cre;Wnt10a*$^{flox/flox}$ mice. Blue lines circle the dental mesenchymal cells adjacent to the HERS cells in the root furcation region. Scale bars: 20 μm. (**C**) Volcano plot of the differentially expressed Wnt pathway genes detected by RNA-sequencing from M1 of *Wnt10a*$^{flox/flox}$ and *K14-Cre;Wnt10a*$^{flox/flox}$ mice. The vertical dashed line shows a threshold of up- and downfold changes, and the horizontal dashed line represents a *P* value of 0.05. All Wnt family ligands with statistically significant differences are pointed out. Up- and downregulated genes ($P<0.05$) are depicted in red spots and green spots, respectively. The genes with no statistically significant differences are depicted in gray spots. (**D**) Log2 (FPKM value) values of Wnt ligands detected by RNA-sequencing from M1 of *Wnt10a*$^{flox/flox}$ and *K14-Cre;Wnt10a*$^{flox/flox}$ mice are encoded in the heat map from low expression (blue) to high expression (red). *Wnt4* is framed and highlighted in green. (**E**, **F**) Quantitative reverse transcription polymerase chain reaction of all the Wnt ligands expressed in the first mandibular molars of *Wnt10a*$^{flox/flox}$ and *K14-Cre;Wnt10a*$^{flox/flox}$ mice at postnatal day 4. The expression level of *Wnt6* from *Wnt10a*$^{flox/flox}$ samples is set as 1 for the relative expression. Values are presented as mean ± SD. $^{*}P<0.05$, $^{**}P<0.01$. $n=3$ per group. DE, dental epithelium; HERS, Hertwig's epithelial root sheath; FPKM, fragments per kilobase of exon model per million mapped reads; M1, first mandibular molar.

the sagittal plane (Fig. 5C), and 2 independent oval profiles of the roots in the axial plane (Fig. 5E$_1$–E$_3$), whereas the control-shRNA-infected *K14-Cre;Wnt10a*$^{flox/flox}$ molars all presented taurodontism (n = 6), with the absence of root furcation in the sagittal plane (Fig. 5F) and 1 whole oval root profile in the axial plane (Fig. 5H$_1$–H$_3$). In the *Wnt4*-shRNA-infected *K14-Cre;Wnt10a*$^{flox/flox}$ molars, an isthmus in the middle resembling root furcation appeared after kidney capsule transplantation (n = 5 in 6 treated samples; Fig. 5I). Specifically, the normal apical growth of the roots was not disturbed (Fig. 5J), and the root profile changed from oval to peanut shaped in the axial planes of *Wnt4*-shRNA-infected *K14-Cre;Wnt10a*$^{flox/flox}$ molars (Fig. 5K$_1$–K$_3$). Taken together, our results indicate that in *K14-Cre;Wnt10a*$^{flox/flox}$-sh*Wnt4* molars, the suppression of elevated *Wnt4* partially inhibited the overgrowth of dental pulp in the furcation and ameliorated the taurodontism.

Discussion

Tooth root development, growth, and regeneration are governed by the precise regulation of signaling networks. For the first time, we reveal that epithelial *Wnt10a* but not mesenchymal *Wnt10a* is essential for the proper formation of root furcation, and we demonstrate that epithelial *Wnt10a* plays a crucial role in controlling the organized proliferation of adjacent mesenchymal cells by regulating proper mesenchymal *Wnt4* expression during root furcation morphogenesis.

A previous study showed that *Wnt10a* is highly expressed in the epithelial cells of the crown and its underlying mesenchymal cells, but it is mainly expressed in the preodontoblasts adhering to HERS during root development (Yamashiro et al. 2007). Interestingly, our RNAscope results showed dynamic *Wnt10a* expression in the epithelial and mesenchymal cells of the root furcation, thus demonstrating the crucial role of *Wnt10a* in guiding the root furcation formation.

HERS are formed by the continuous extension of inner and outer enamel epithelium at the cervical loop in the tooth crown (Huang and Chai 2012). Since PN4, when the crown is fully developed and the root is just beginning to develop, a horizontal elongation of HERS cells leads to a closure of the pulp chamber floor and the subsequent formation of root furcation (Liu et al. 2015; Li et al. 2017). In our study, the proliferation of epithelial cells is compromised in *K14-Cre;Wnt10a*$^{flox/flox}$ mice; HERS cannot elongate horizontally to guide the normal formation of pulp chamber floor; and tooth displays an absence of or apically located root furcation. This result provides solid evidence for the epithelial guidance of multiroot tooth morphogenesis and further suggests the pivotal role of epithelial *Wnt10a* in regulating the proper molar root pattern.

Tooth root development, as a later stage of tooth development, is mediated by epithelial-mesenchymal interactions (Li et al. 2017; Jing et al. 2019). Proliferating mesenchymal cells

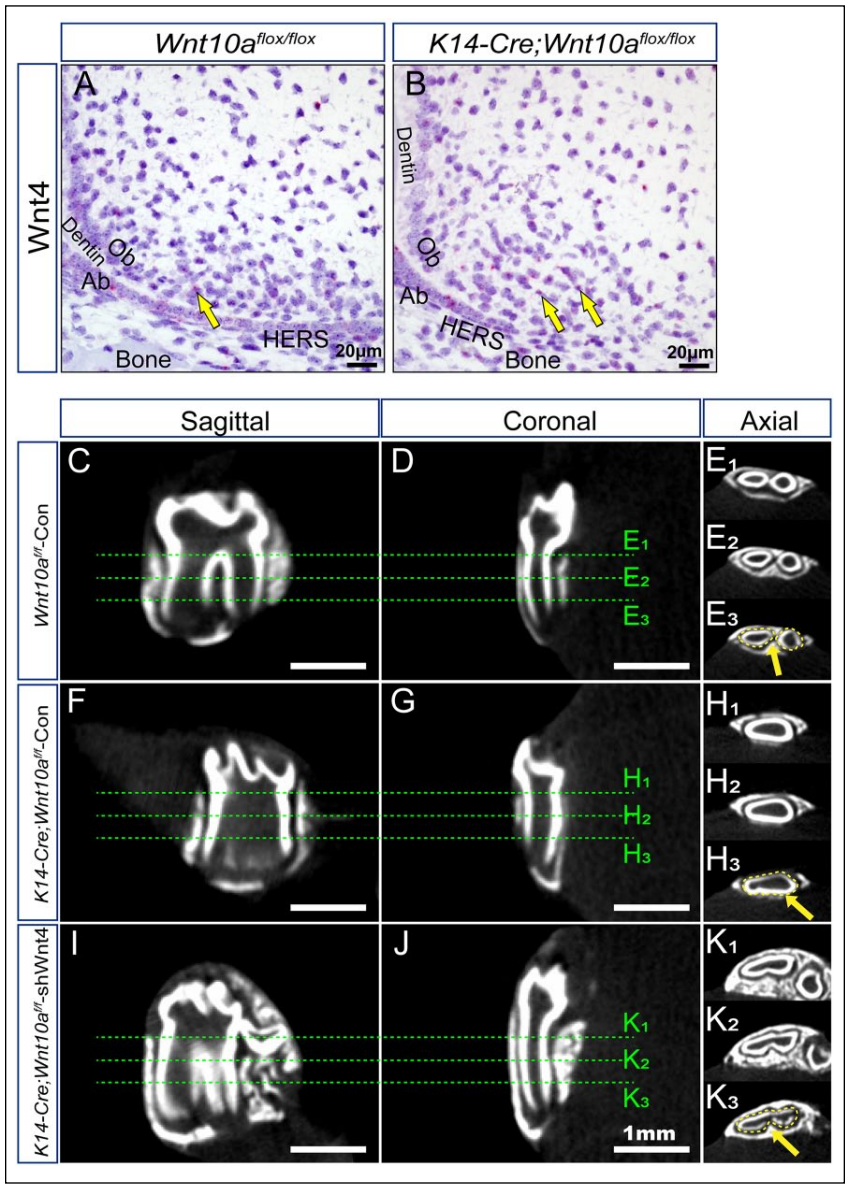

Figure 5. Compensatory upregulation of *Wnt4* contributes to the increased dental pulp proliferation and taurodontism in *K14-Cre;Wnt10a*$^{flox/flox}$ mice. (**A**, **B**) RNAscope in situ hybridization of *Wnt4* expression in the furcation region of first mandibular molars from *Wnt10a*$^{flox/flox}$ and *K14-Cre;Wnt10a*$^{flox/flox}$ mice on coronal section. Yellow arrows indicate the *Wnt4* positive signal. Scale bars: 20 μm. (**C–K**) Micro–computed tomography scanning images of *Wnt10a*$^{flox/flox}$ molars infected with control-shRNA, *K14-Cre;Wnt10a*$^{flox/flox}$ molars infected with control-shRNA, and *K14-Cre;Wnt10a*$^{flox/flox}$ molars infected with *Wnt4*-shRNA. Sagittal view in the middle and coronal view in the mesial root of molars from 3 groups. ($E_{1\text{-}3}$, $H_{1\text{-}3}$, $K_{1\text{-}3}$) Axial view of the upper, middle, and lower one-third of the roots from 3 groups. Arrows indicate the root furcation region; dashed lines indicate the root contour. $n \geq 6$ per group. Scale bars: 1 mm. Ab, ameloblasts; Ob, odontoblasts.

adhered to HERS are involved in epithelial cell migration, which is essential for normal root formation (Sohn et al. 2014). Our results show a significant increase of dental pulp mesenchymal cell proliferation of the presumptive root furcating region in *K14-Cre;Wnt10a*$^{flox/flox}$ mice, suggesting that taurodontism is caused by reduced HERS cell proliferation at the initial stage of root development as well as excessive proliferation of adjacent mesenchymal cells in dental papilla during root development. However, the proliferation of dental follicle cells did not show a significant difference in the alveolar bone between *Wnt10a*$^{flox/flox}$ and *K14-Cre;Wnt10a*$^{flox/flox}$ mice. The functional significance of *Wnt10a* on the relationship of alveolar bone development and root furcation formation needs to be further investigated.

Including *Wnt10a*, a number of Wnt ligands are expressed continuously during tooth development (de Lau et al. 2014). In our *K14-Cre;Wnt10a*$^{flox/flox}$ mice, an elevated *Axin2* is observed in the dental pulp. Moreover, RNA-seq, RT-qPCR, and RNAscope results show that *Wnt4* expression is significantly increased in *K14-Cre;Wnt10a*$^{flox/flox}$ mouse molars. Furthermore, knockdown of *Wnt4* in the molar germ of *K14-Cre;Wnt10a*$^{flox/flox}$ mice at PN4, which is the key time point for root initiation, ameliorates taurodontism. Our data indicate that knockout of epithelial-*Wnt10a* results in the compensatory upregulation of *Wnt4* and elevated Wnt/β-catenin signaling in the mesenchyme of apical papilla, thus leading to the increased proliferation and overgrowth of dental pulp in root furcation, which might contribute to taurodontism.

Our study provides in vivo evidence that epithelial *Wnt10a* guides root furcation formation. Insights into the epithelial-mesenchymal interaction driven by *Wnt10a* will greatly enhance our understanding of the molecular and cellular mechanisms involved in normal and abnormal tooth root development. Information from this study may facilitate bioengineered root regeneration.

Author Contributions

M. Yu, Y. Liu, contributed to data acquisition, analysis, and interpretation, drafted the manuscript; Y. Wang, contributed to data acquisition and analysis, drafted the manuscript; S.W. Wong, contributed to data analysis, critically revised the manuscript; J. Wu, contributed to data acquisition, drafted the manuscript; H. Liu, contributed to data interpretation, drafted the manuscript; H. Feng, contributed to conception, critically revised the manuscript; D. Han, contributed to conception and design, critically revised the manuscript. All authors gave final approval and agree to be accountable for all aspects of the work.

Acknowledgments

We thank Prof. Yang Chai at University of Southern California for careful reading of the manuscript, and Shaohua Zhan for plotting the Volcano chart in Figure 4. This work was supported by the National Natural Science Foundation of China (grants 81970902, 81771054, and 81600846). The authors declare no potential conflicts of interest with respect to the authorship and/or publication of this article.

ORCID iD

D. Han https://orcid.org/0000-0001-9625-3384

References

Adaimy L, Chouery E, Megarbane H, Mroueh S, Delague V, Nicolas E, Belguith H, De MP, Megarbane A. 2007. Mutation in WNT10A is associated with an autosomal recessive ectodermal dysplasia: the odonto-onychodermal dysplasia. Am J Hum Genet. 81(4):821–828.

Brault V, Moore R, Kutsch S, Ishibashi M, Rowitch DH, McMahon AP, Sommer L, Boussadia O, Kemler R. 2001. Inactivation of the beta-catenin gene by Wnt1-Cre-mediated deletion results in dramatic brain malformation and failure of craniofacial development. Development. 128(8):1253–1264.

Byrne C, Tainsky M, Fuchs E. 1994. Programming gene expression in developing epidermis. Development. 120(9):2369–2383.

Dassule HR, McMahon AP. 1998. Analysis of epithelial-mesenchymal interactions in the initial morphogenesis of the mammalian tooth. Dev Biol. 202(2):215–227.

de Lau W, Peng WC, Gros P, Clevers H. 2014. The R-spondin/Lgr5/Rnf43 module: regulator of Wnt signal strength. Genes Dev. 28(4):305–316.

He H, Han D, Feng H, Qu H, Song S, Bai B, Zhang Z. 2013. Involvement of and interaction between WNT10A and EDA mutations in tooth agenesis cases in the Chinese population. PloS One. 8(11):e80393.

Huang XF, Chai Y. 2012. Molecular regulatory mechanism of tooth root development. Int J Oral Sci. 4(4):177–181.

Jing J, Feng J, Li J, Han X, He J, Ho TV, Du J, Zhou X, Urata M, Chai Y. 2019. Antagonistic interaction between Ezh2 and Arid1a coordinates root patterning and development via Cdkn2a in mouse molars. Elife. 8:e46426.

Kantaputra P, Sripathomsawat W. 2011. WNT10A and isolated hypodontia. Am J Med Genet A. 155(5):1119–1122.

Lakso M, Pichel JG, Gorman JR, Sauer B, Okamoto Y, Lee E, Alt FW, Westphal H. 1996. Efficient in vivo manipulation of mouse genomic sequences at the zygote stage. Proc Natl Acad Sci U S A. 93(12):5860–5865.

Li J, Huang X, Xu X, Mayo J, Bringas P Jr, Jiang R, Wang S, Chai Y. 2011. SMAD4-mediated WNT signaling controls the fate of cranial neural crest cells during tooth morphogenesis. Development. 138(10):1977–1989.

Li J, Parada C, Chai Y. 2017. Cellular and molecular mechanisms of tooth root development. Development. 144(3):374–384.

Liu Y, Feng J, Li J, Zhao H, Ho TV, Chai Y. 2015. An Nfic-hedgehog signaling cascade regulates tooth root development. Development. 142(19):3374–3382.

Petrof G, Fong K, Lai-Cheong JE, Cockayne SE, McGrath JA. 2011. Schopf-Schulz-Passarge syndrome resulting from a homozygous nonsense mutation, p.Cys107X, in WNT10A. Australas J Dermatol. 52(3):224–226.

Sohn WJ, Choi MA, Yamamoto H, Lee S, Lee Y, Jung JK, Jin MU, An CH, Jung HS, Suh JY, et al. 2014. Contribution of mesenchymal proliferation in tooth root morphogenesis. J Dent Res. 93(1):78–83.

Song S, Zhao R, He H, Zhang J, Feng H, Lin L. 2014. WNT10A variants are associated with non-syndromic tooth agenesis in the general population. Hum Genet. 133(1):117–124.

Thesleff I. 2003. Epithelial-mesenchymal signalling regulating tooth morphogenesis. J Cell Sci. 116(Pt 9):1647–1648.

van den Boogaard MJ, Creton M, Bronkhorst Y, van der Hout A, Hennekam E, Lindhout D, Cune M, Ploos van Amstel HK. 2012. Mutations in WNT10A are present in more than half of isolated hypodontia cases. J Med Genet. 49(5):327–331.

van Genderen C, Okamura RM, Farinas I, Quo RG, Parslow TG, Bruhn L, Grosschedl R. 1994. Development of several organs that require inductive epithelial-mesenchymal interactions is impaired in LEF-1-deficient mice. Genes Dev. 8(22):2691–2703.

Verstraeten B, Sanders E, van Hengel J, Huysseune A. 2010. Zebrafish teeth as a model for repetitive epithelial morphogenesis: dynamics of e-cadherin expression. BMC Dev Biol. 10:58.

Wang F, Flanagan J, Su N, Wang LC, Bui S, Nielson A, Wu X, Vo HT, Ma XJ, Luo Y. 2012. RNAscope: a novel in situ RNA analysis platform for formalin-fixed, paraffin-embedded tissues. J Mol Diagn. 14(1):22–29.

Wu X, Hu L, Li Y, Li Y, Wang F, Ma P, Wang J, Zhang C, Jiang C, Wang S. 2018. SCAPS regulate differentiation of DFSCs during tooth root development in swine. Int J Med Sci. 15(4):291–299.

Xu M, Horrell J, Snitow M, Cui J, Gochnauer H, Syrett CM, Kallish S, Seykora JT, Liu F, Gaillard D, et al. 2017. WNT10A mutation causes ectodermal dysplasia by impairing progenitor cell proliferation and KLF4-mediated differentiation. Nat Commun. 8:15397.

Yamashiro T, Zheng L, Shitaku Y, Saito M, Tsubakimoto T, Takada K, Takano-Yamamoto T, Thesleff I. 2007. Wnt10a regulates dentin sialophosphoprotein mRNA expression and possibly links odontoblast differentiation and tooth morphogenesis. Differentiation. 75(5):452–462.

Yang J, Wang SK, Choi M, Reid BM, Hu Y, Lee YL, Herzog CR, Kim-Berman H, Lee M, Benke PJ, et al. 2015. Taurodontism, variations in tooth number, and misshapened crowns in Wnt10a null mice and human kindreds. Mol Genet Genomic Med. 3(1):40–58.

Yu M, Liu Y, Liu H, Wong SW, He H, Zhang X, Wang Y, Han D, Feng H. 2019. Distinct impacts of bi-allelic WNT10A mutations on the permanent and primary dentitions in odonto-onycho-dermal dysplasia. Am J Med Genet A. 179(1):57–64.

Yu M, Wong SW, Han D, Cai T. 2019. Genetic analysis: Wnt and other pathways in nonsyndromic tooth agenesis. Oral Dis. 25(3):646–651.